The 2019 World Congress on
Advances in Structural Engineering and Mechanics (ASEM19)
Jeju Island, Korea, September 17 - 21, 2019

In-Plane Cyclic Loading Behavior of Corner Steel-Reinforced Composite Walls

*Hyeon-Jin Kim[1)] and Hong-Gun Park[2)]

[1),2)] *Department of Architectural Engineering, SNU, Seoul, 08826, Korea*
[1)] *bultanun2@gmail.com*

ABSTRACT

For better structural performance and constructability, a novel composite wall method using steel plates at the corners of the core section was developed. To verify the flexural capacity of the proposed method, cyclic loading tests were performed for conventional reinforced concrete wall specimens and corner steel-reinforced concrete (CSRC) composite wall specimens. The test results showed that, when the same amount of steel was used, the use of the corner steel plates increased the flexural stiffness, ductility and energy dissipation capacity of the specimens. The flexural strength of the CSRC specimens was safely predicted by existing design methods.

1. INTRODUCTION

For structural walls in nuclear plants or high-rise buildings, the use of steel-concrete (SC) composite walls (**Fig. 1**) has increased for their great structural performance and constructability. In the beginning, reinforced concrete (RC) panels were frequently used for infilled walls between beam-column steel frames, to provide robust design for earthquake and wind loads. For better application to high-rise buildings, concrete-encased steel plates across the wall cross section were used, to provide greater shear resistance, resiliency, and to reduce the wall thickness. The steel plates were usually welded to the boundary elements, such as concrete-filled steel tube (CFST) columns and wide flange section steel columns. However, despite such structural advantages, the field work for re-bars, concrete forms, and temporary supports has remained, which decreased the constructability. More recently, composite walls using faceplates located at the wall surface (double skin composite wall, DSC wall) has been growing option for nuclear plant structures. Because the faceplates can act as concrete forms, the labor cost and construction time can be significantly saved. To investigate the structural performances, in terms of in-plane, out-of-plane, shear, and flexural behaviors of the DSC walls, various experimental studies were performed for

---

[1)] Graduate Student
[2)] Professor

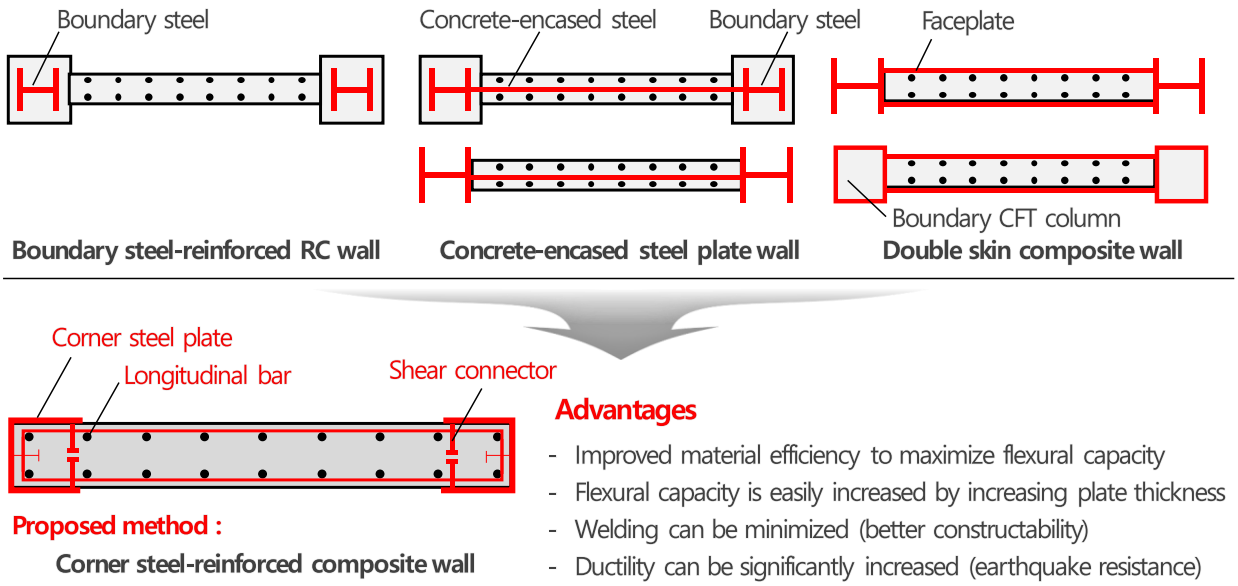

Fig. 1 Steel-concrete (SC) composite walls

isolated walls or coupled walls (Mckinley and Boswell 2002; Clubley et al. 2013; Zhao and Astaneh-Asl 2004; Eom et al. 2009; Ji et al. 2013; and Lin Chen et al. 2015; Varma et al. 2015; and Ji et al. 2017). The test results showed the increases of strength and ductility of the DCS walls, which confirmed the good applicability in high-rise buildings. However, since the core walls in high-rise buildings generally consist of various exterior and interior wall segments, the existing methods may require significant amounts of steel and weld work between the steel components.

For better constructability and economy, a new SC composite (corner steel-reinforced concrete, CSRC) walls using steel plates at the corners of the cross section was developed. Because the steel area is concentrated at the section corners, the material efficiency to maximize the flexural capacity can be improved. In addition, the number of weld connections required between the steel plates can be reduced, which improves the constructability. When compared to the DSC walls, although the proposed method requires the field work of concrete forms, the required area for fire-proofing can be reduced.

In this study, two conventional RC structural wall specimens and two CSRC wall specimens were tested to investigate the effect of the corner steel plates on the flexural capacity of the walls. From the test results, the structural capacities including load-carrying capacity, deformation capacity (ductility), and energy dissipation capacity were evaluated, and compared with the prediction of existing design method.

2. TEST PLAN

2.1 test specimens

Table 1 and **Fig. 2** show the geometric configuration and material properties of the conventional RC wall specimens (**RC1** and **RC2**) and CSRC wall specimens (**CS1** and **CS2**). The dimensions of the wall cross section were length x thickness = 1800 mm

x 300 mm, and the clear height of the wall specimens was 4,500mm (height-to-length ratio = 2.5). For **RC1**, **RC2**, and **CS1**, the steel ratio was 3.3%. In the case of **CS2**, the steel ratio was increased to 5.5%, by increasing the steel plate thickness. In **RC1**, longitudinal D35 bars (F_y = 519 MPa) were uniformly placed at a spacing of 210 mm. In **RC2**, nine longitudinal bars (D35) were concentrated at wall boundaries, at a spacing of 100 mm. The special boundary elements (hoop bars D13 at 75 mm-spacing for 1950 mm distance above the wall base; D13 at 150 mm-spacing for the remaining height) were used at the compression zones, to be designed as special structural walls specified in ACI 318-19 (2019). Longitudinal D16 bars (at 420 mm spacing, F_y = 445 MPa) were used for the web reinforcement. In CSRC wall specimen **CS1**, channel-shaped steel plates (C-300x300x9, F_y = 379 MPa) were placed at the surface of the wall boundaries. For composite action between the steel plates and concrete, six shear studs were welded to the plates at a vertical spacing of 150 mm. In the wall web, longitudinal D16 bars (F_y = 445 MPa) were placed at a spacing of 412.5 mm, which satisfied the maximum spacing of ACI 318-19 (2019). In **CS2**, the thickness of the steel plates (C-300x300x16, F_y = 291 MPa) was increased to 16 mm. The other structural details are the same as those of **CS1**. For all specimens, transverse D16 bars (F_y = 445 MPa) were used at a vertical spacing of 150 mm (transverse bar ratio = 0.88%).

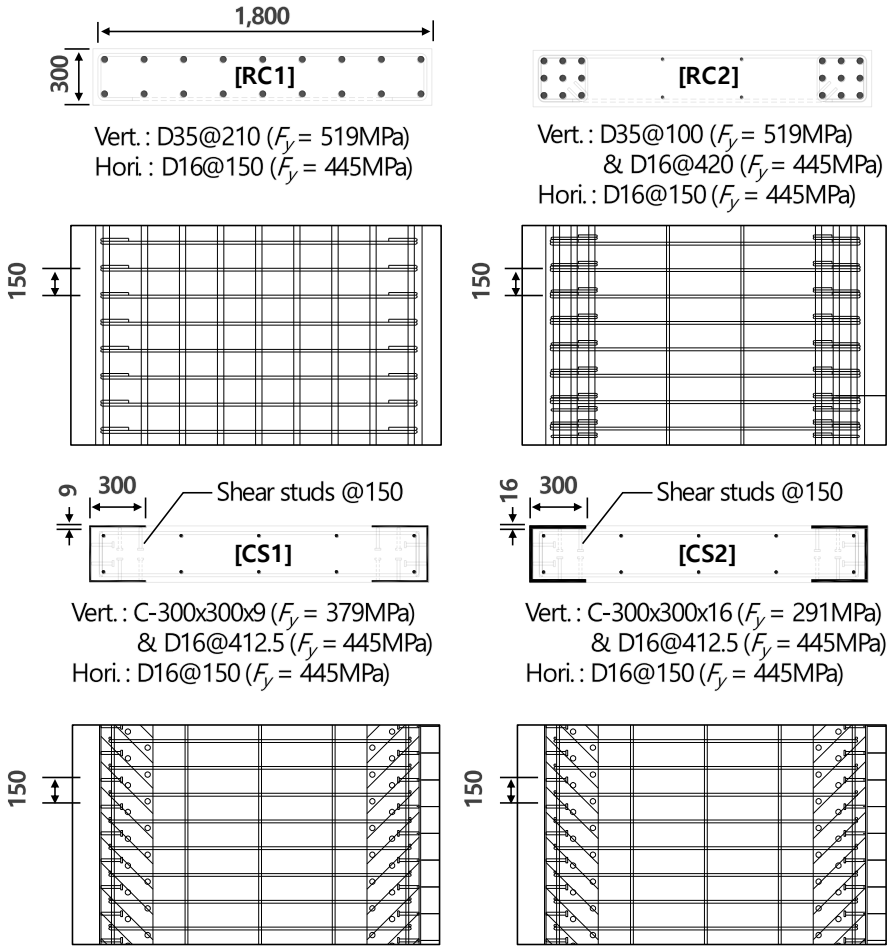

Fig. 2 Cross sections of test specimens (unit: mm)

Table 1. Test parameters of specimens

Specimens	RC1	RC2	CS1	CS2
Wall type	Reinforced concrete	Reinforced concrete	Corner steel-reinforced concrete	Corner steel-reinforced concrete
Concrete strength (MPa)	64.6	68.2	68.2	68.2
Longitudinal steel @spacing, mm (yield strength, MPa)	D35@210 (519)	D35@100 (519) (boundary bar) / D16@420 (445) (web bar)	C-300x300x9 (379) / D16@412.5 (445)	C-300x300x16 (291) / D16@412.5 (445) (web bar)
Longitudinal steel ratio (%)	3.3	3.3	3.3	5.5
Transverse bar @spacing, mm (yield strength, MPa)	D16@150 (445)	D16@150 (445)	D16@150 (445)	D16@150 (445)
Transverse bar ratio (%)	0.88	0.88	0.88	0.88

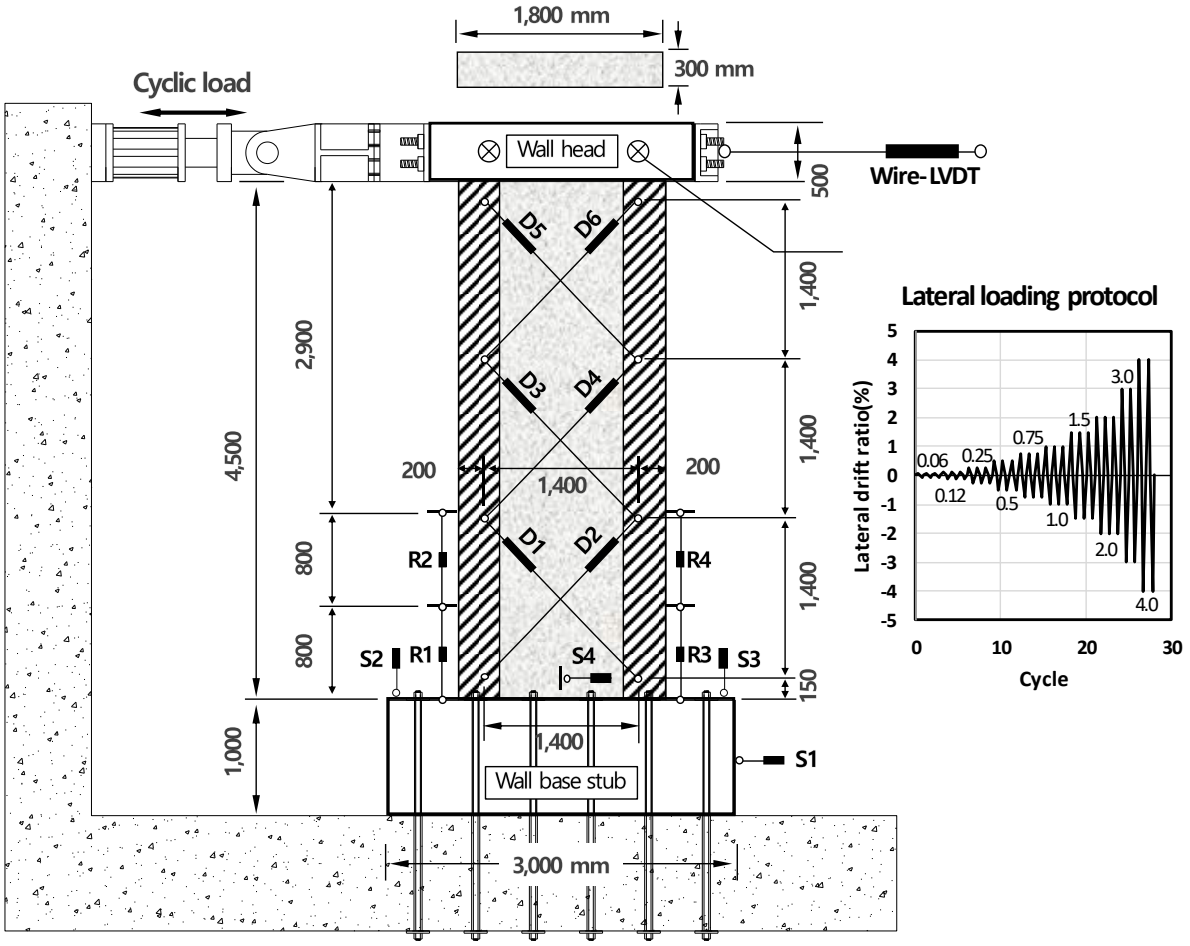

Fig. 3 Test and measurement setup

2.2 Test setup

Fig. 3 shows the test setup for cyclic lateral loading. Using a 3MN-actuator, lateral load was applied to the top of the wall specimens, under displacement control. The cyclic loading protocol followed the specification in ACI 374 (2013). The numbers of load cycles were three times at lateral drift ratios δ = 0.06, 0.12, 0.25, 0.5, 0.75, 1.0, 1.5, and 2.0%; two times at δ = 3.0 and 4.0%. An axial force was neglected in the test, because the maximum capacity of the actuator was not sufficient to affect the structural capacity of the full-scale test specimens. At the bottom of the wall specimens, 2m-long anchor bolts (diameter = 48 mm) were pre-tensioned between the wall base stub and the reaction slab in the laboratory.

During the test, the lateral displacement was measured using a wire-type LVDT at the top of the wall specimens. The flexural deformation of the plastic hinge region was measured using bar-type LVDTs that were installed in a 1600mm-distance from the wall base, at the left and right sides of the specimens. The shear distortion of the web wall was measured using X-braced LVDTs that were divided into three regions along the wall height. To evaluate the net lateral displacement, the contributions of base sliding, wall sliding, and rocking to the lateral displacement were subtracted from the lateral displacement.

3. TEST RESULTS

3.1 Lateral load – drift ratio relationship and failure mode

Fig. 4 shows the lateral load-drift ratio (P-δ) relationships of the wall specimens, while **Fig. 5** presents the failure modes of the concrete and steel at the end of the tests. The drift ratio was determined by dividing the net lateral displacement Δ by the effective height of the specimens (H_e = 4,750 mm). **Table 2** presents the peak strength P_u, yield stiffness K_y, yield drift ratio δ_y, and ultimate drift ratio δ_u of the test specimens. The yield stiffness K_y was determined as the slope connecting the origin to 0.75P_u point in the backbone curve. The yield drift ratio was defined as $\delta_y = P_u / (K_y H_e)$. The ultimate drift ratio δ_u was the maximum drift ratios satisfying the post-peak strength greater than 0.75P_u.

Fig. 4(a) shows the test result of RC specimen **RC1**. After tensile yielding of the longitudinal bars, the crushing of the cover concrete occurred at the compression zone (wall boundary). The peak strengths P_u = +1299 kN and -1273kN were then developed at drift ratios of +1.62 % and -1.27 %, respectively. After the peak strength, spalling of the cover concrete occurred, which decreased the load-carrying capacity. At a drift ratio of -2.5 %, the longitudinal bars at the wall boundary showed local buckling (**Fig. 5**(a)). The ultimate drift ratios were δ_u = +2.62 % and -2.77 %. As shown in **Fig. 4**(b), the peak strengths of **RC2** were increased to P_u = +1466 kN (at 1.11 %) and -1445kN (at -1.70 %), due to the concentrated re-bar area at the wall boundary. After the peak strength, horizontal cracking gradually increased at the bottom of the wall (**Fig. 5**(b)), due to the minimum ratio of longitudinal re-bars in the web wall. As the drift ratio increased to negative 3.0 %, shear sliding occurred, which significantly decreased the lateral stiffness. Ultimately, the ultimate drift ratios were δ_u = +2.73 % and -1.71 %.

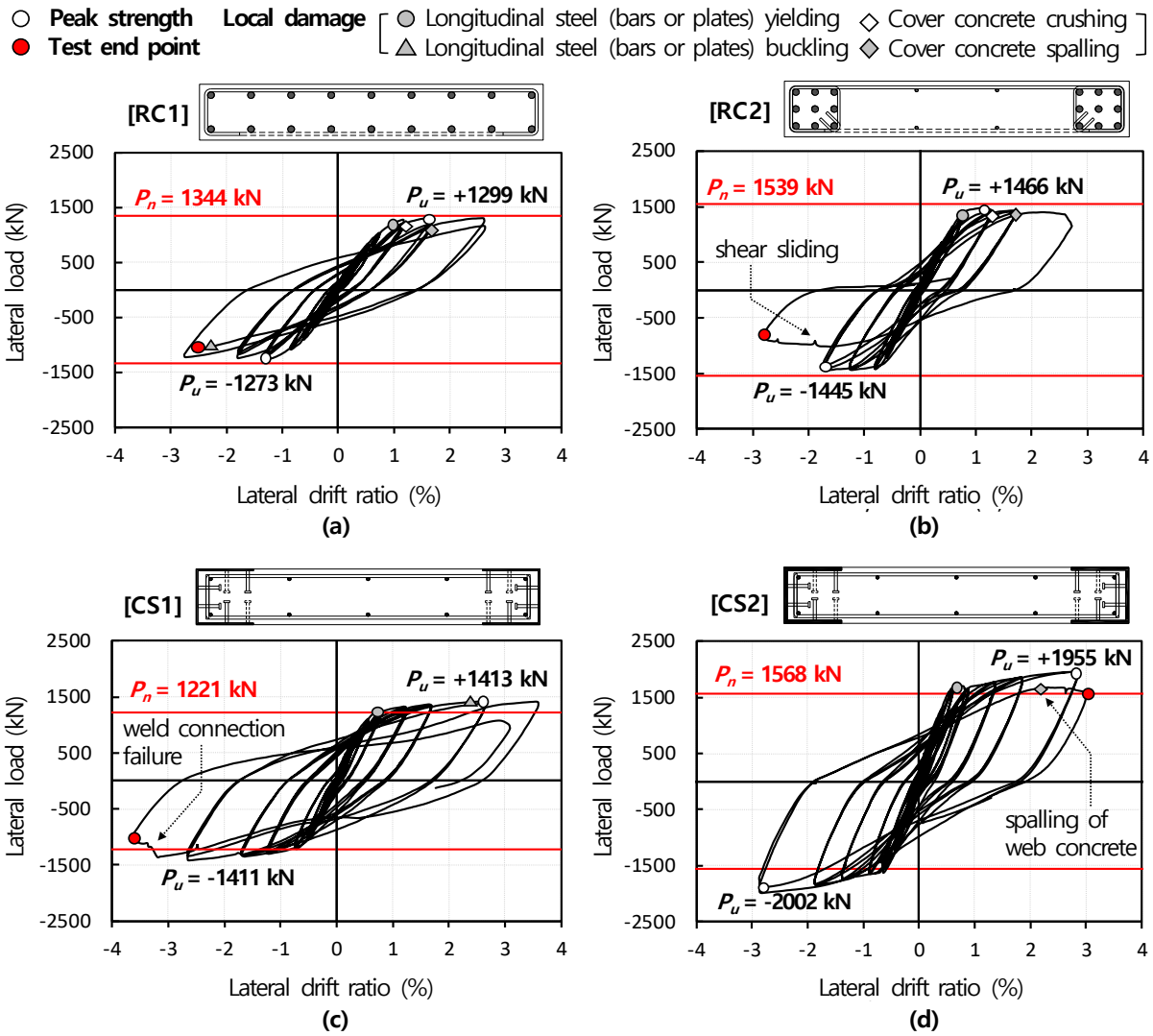

Fig. 4 Lateral load-drift ratio relationships of specimens

Table 2. Test results (positive direction / negative direction)

Specimens	Test strength P_u (kN)	Yield drift ratio δ_y (%)	Ultimate drift ratio δ_u (%)	Yield stiffness K_y (kN/mm)	Ductility (δ_u/δ_y)	Nominal strength P_n (kN)
RC1	1299/-1273	0.94/-0.94	2.62/-2.77	29.4/28.9	2.79/2.96	1344
RC2	1466/-1445	0.80/-0.72	2.73/-2.80	39.0/42.5	3.41/3.87	1539
CS1	1413/-1411	0.77/-0.84	3.59/-3.63	39.2/35.8	4.68/4.33	1221
CS2	1955/-2002	0.72/-0.78	2.99/-2.87	58.1/54.6	4.18/3.68	1568

Figs. 4(c) and (d) show the test results of CSRC specimens **CS1** and **CS2**. Because the corner steel plates confined the concrete at the wall boundaries, the crushing or spalling of the concrete were not clearly seen in the tests (The concrete

spalling was only observed in the web wall of **CS2**). Despite the yielding of the corner steel plates, the load-carrying capacity linearly increased until the last loading step. Consequently, the drift ratios corresponding to the peak strength were 2.59 % and -2.64 % for **CS1**; 2.82 % and -2.83 % for **CS2**, which were much greater than those of the RC specimens. This result is attributed to the combined effect of the lateral confinement to the concrete and strain hardening of the corner steel plates. For this reason, the ultimate drift ratios (3.59 % and -3.63 % for CS1; 2.99 % and – 2.87 % for CS2) were slightly greater than those of the RC specimens. In **CS1**, despite the local buckling of the corner steel plates approximately at 2.0%, the strength degradation was not significant. The test was finished, because the strength was significantly degraded due to the weld-fracture of the vertical connection between the corner steel plates (located at 2000 mm above the wall base, **Fig. 5**(c)). In **CS2**, the spalling of the web concrete significantly occurred at the second cycle of the last loading step (**Fig. 5**(d)), which decreased the strength and stiffness. The steel plate buckling did not occur until the end of the test. For both CSRC specimens, shear sliding did not occur despite the minimum ratio of the longitudinal bar in the web wall, due to the large shear resistance of the corner steel plates.

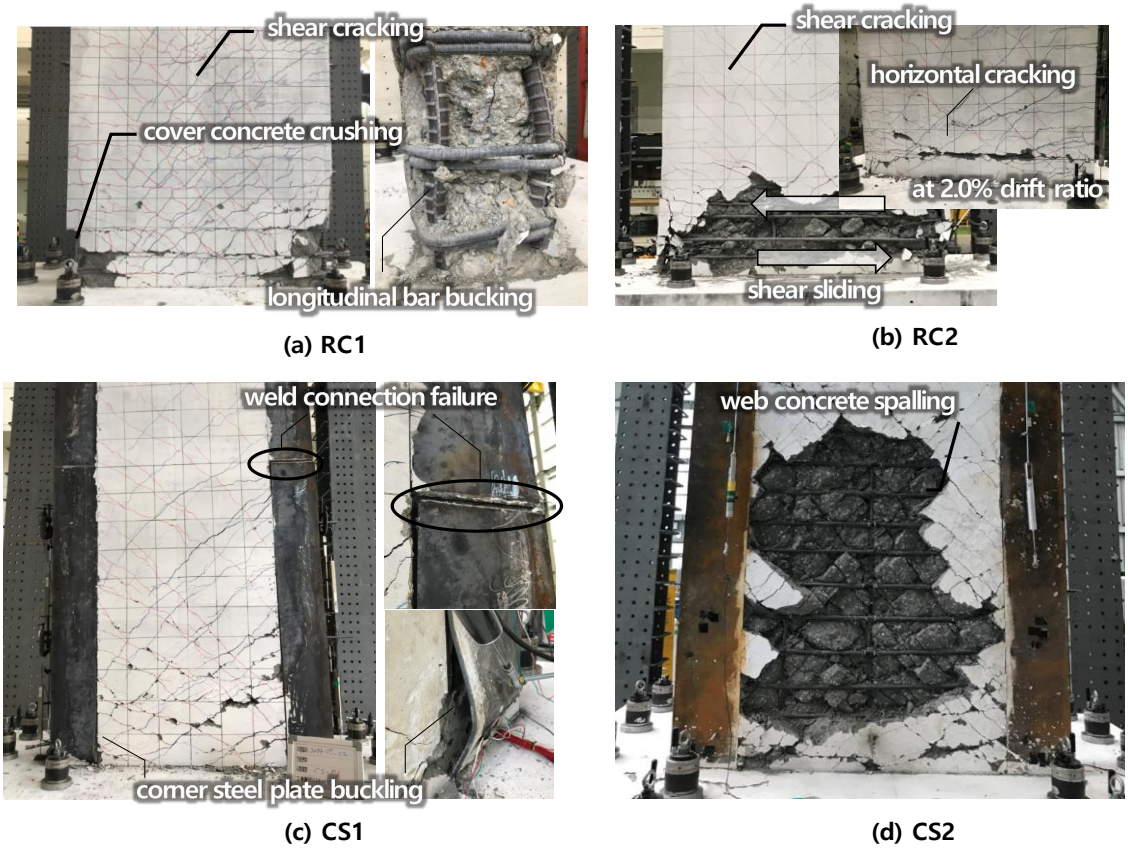

Fig. 5 Damages of concrete and steel at the end of tests

3.2 Flexural strength, stiffness, and ductility

Table 2 shows the nominal flexural strength of the specimens, which were predicted according to ACI 318 (2019). The peak strengths of **RC1** and **RC2** were

slightly less than those from the predictions (1344 kN for **RC1** and 1539 kN for **RC2**). In the case of **CS1** and **CS2**, the test strengths were 16 % and 25 % greater than the prediction, respectively, due to the better contribution of the corner steel plates to the flexural strength. The test strength of **CS1** was slightly less than that of **RC2** with the same steel ratio, due to the lower yield strength of steel (= 379 MPa) than that of re-bars (= 519 MPa) in **RC2**. In **RC2** and **CS1** with the large steel area at the wall boundary, the yield stiffness was similar, while **RC1** showed the lowest stiffness. In the case of **CS2** with increased steel ratio, the yield stiffness was almost twice as that of **RC1**. In **CS1** and **CS2**, the ductility (defined as δ_u / δ_y) was greater than that of **RC1** and **RC2**, due to the corner steel plates.

3.3 Energy dissipation capacity

Fig. 5 shows the dissipated energy per load cycle, varying with the lateral drift ratio. The dissipated energy for an incremental step was defined as the enclosed area of first cycle in the lateral load-drift ratio relationship. For all specimens, the dissipated energy significantly increased after the drift ratio of 1.0% corresponding the yielding of the longitudinal steel. In general, the dissipated energy of the CSRC specimens was greater than that of the RC specimens, due to the increased strength and deformation capacity.

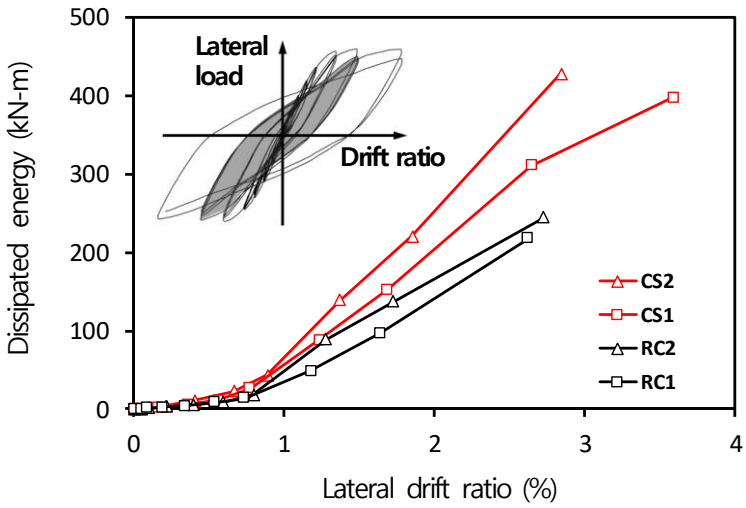

Fig. 6 Dissipated energy-drift ratio relationships of specimens

4. SUMMARY AND CONCLUSIONS

In this study, cyclic lateral loading tests were performed to investigate the structural capacity of the newly developed CSRC walls. From the test results, the load-carrying capacity, deformation capacity, failure mode, and energy dissipation capacity were investigated. The main conclusions are presented as follows:

(1) The flexural strength of the CSRC wall specimens can be safely predicted by existing design method ACI 318-19.

(2) By using the steel plates (with the same amount of steel in RC specimens) at

the surface of the wall boundary, the lateral load-resisting stiffness can be comparable to that of the RC wall designed as special structural walls using special boundary elements, specified in ACI 318-19. When the steel ratio was increased by 67% (using thicker steel plates), the stiffness of the CSRC wall was increased by 49%.

(3) In the CSRC specimens, the seismic performances including the deformation capacity, ductility, and energy dissipation capacity was greater than those of the RC specimens, due to the corner steel plates.

(4) In RC specimen with special boundary elements, the minimum ratio of longitudinal bars was used in the web wall. Such configuration induced shear sliding of the web wall in the large inelastic deformation. On the other hand, when corner steel plates were used, the shear sliding was limited due to the large shear resistance of the corner steel plates.

REFERENCES

ACI (American Concrete Institute). (2019), “Building code requirements for structural concrete and commentary.”, *ACI 318-19*, Farmington Hills, MI.

McKinley, B., and Boswell, L. F. (2002). “Behaviour of double skin composite construction.”, *Journal of Constructional Steel Research*, **58**(10), 1347-1359.

Clubley, S. K., Moy, S. S., and Xiao, R. Y. (2003). “Shear strength of steel–concrete–steel composite panels. Part I—testing and numerical modelling.”, *Journal of Constructional Steel Research*, **59**(6), 781-794.

Zhao, Q., and Astaneh-Asl, A. (2004). “Cyclic behavior of traditional and innovative composite shear walls.”, *Journal of Structural Engineering*, **130**(2), 271-284.

Eom, T. S., Park, H. G., Lee, C. H., Kim, J. H., & Chang, I. H. (2009). “Behavior of double skin composite wall subjected to in-plane cyclic loading.”, *Journal of structural engineering*, **135**(10), 1239-1249.

Ji, X., Jiang, F., and Qian, J. (2013). “Seismic behavior of steel tube–double steel plate–concrete composite walls: experimental tests.”, *Journal of Constructional Steel Research*, **86**, 17-30.

Chen, L., Mahmoud, H., Tong, S. M., and Zhou, Y. (2015). “Seismic behavior of double steel plate–HSC composite walls.”, *Engineering Structures*, **102**, 1-12.

Varma, A. H., Malushte, S. R., and Lai, Z. (2015). “Modularity & innovation using steel-plate composite (SC) walls for nuclear and commercial construction.”, *Proceedings of the 11th International Conference on Advances in Steel and Concrete Composite Structures*, Beijing, China (pp. 3-5).

Ji, X., Cheng, X., Jia, X., and Varma, A. H. (2017). “Cyclic in-plane shear behavior of double-skin composite walls in high-rise buildings.”, *Journal of Structural Engineering*, **143**(6), 04017025.